Supporting Information

High performance N-doped carbon nanosheet/MnO_2 cathode derived from bacterial cellulose for aqueous Zn-ion batteries

Wenhai Wang[a,b], Ashley P. Black[b], Cheng Liu[b], Vlad Martin-Diaconescu[c], Laura Simonelli[c], Dino Tonti [b*]

[a]Institute of Clean Energy and Advanced Nanocatalysis (iClean), School of Chemistry and Chemical Engineering, Anhui University of Technology, Maanshan 243002, China

[b]Institut de Ciència de Materials de Barcelona, Consejo Superior de Investigaciones Científicas (ICMAB-CSIC), Campus UAB, ES 08193 Bellaterra, Barcelona, Spain

[c]ALBA Synchrotron Light Source, 08290 Cerdanyola del Vallès, Barcelona, Spain

[*]Corresponding author.
E-mail address: dino.t@csic.es (D. Tonti)

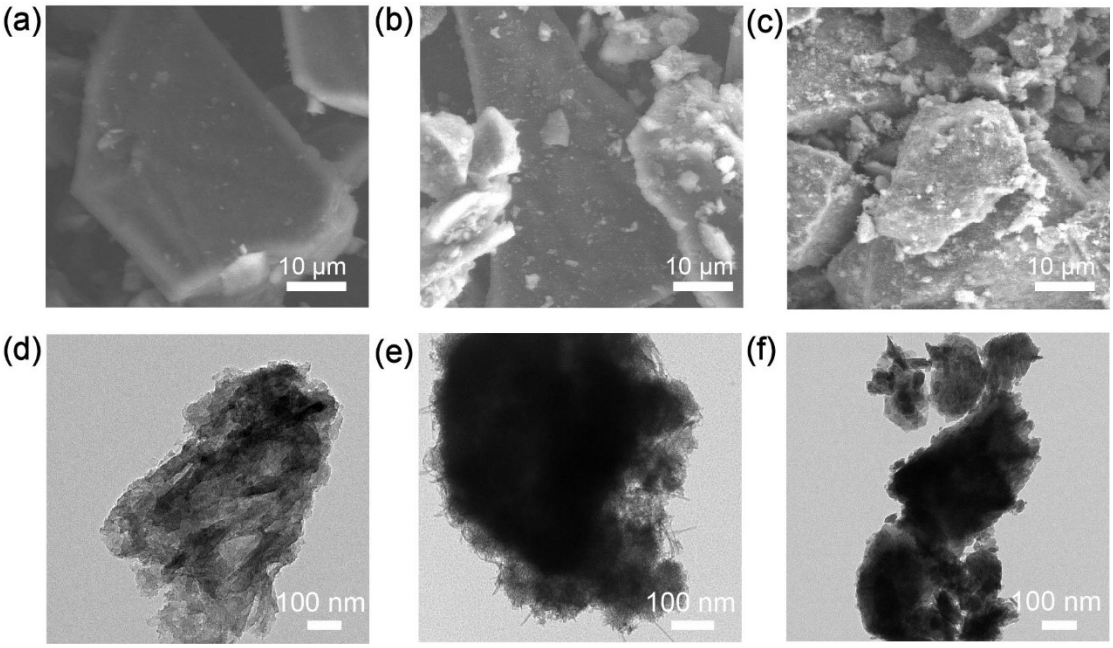

Fig. S1. SEM images of Carbon-w (a), C/MnO_2 (b), Commercial MnO_2 (c). TEM images of Carbon-w (d), C/MnO_2 (e), Commercial MnO_2 (f).

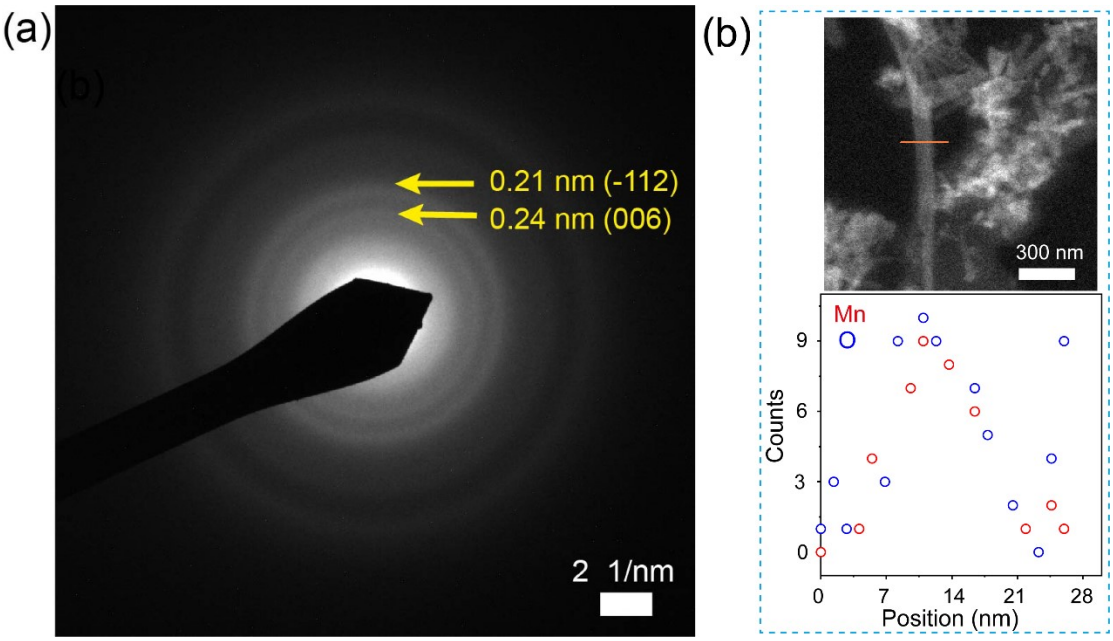

Fig. S2. Transmission electrom mucroscopy of NCS/MnO_2. (a) Selected area electron diffraction (SAED) in the region of Figure 1e. (b) EDS elemental line profiles.

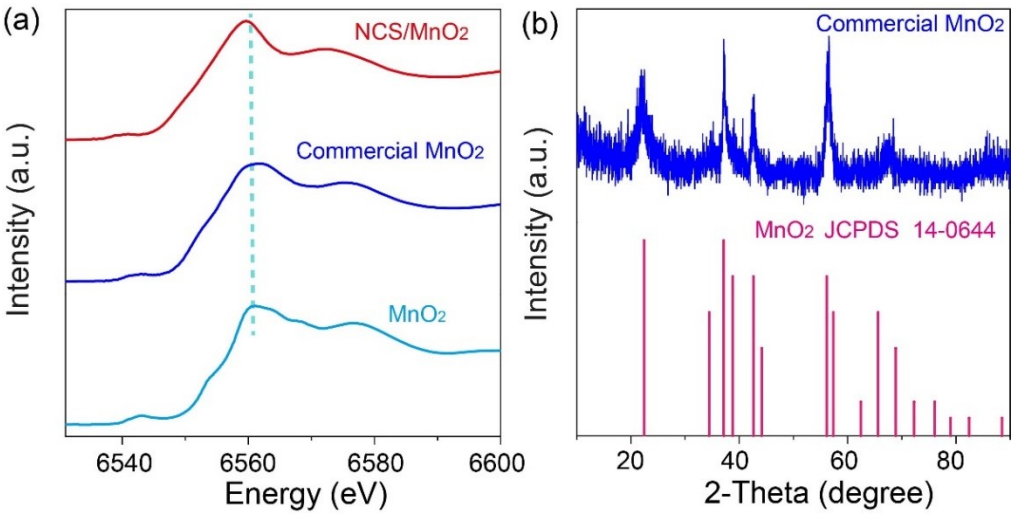

Fig. S3 (a) XAS of NCS/MnO_2, commercial MnO_2 and reference MnO_2; (b) XRD pattern of commercial MnO_2.

Although the energy position of Mn peak for commercial MnO_2 is also close to reference MnO_2, there are some small difference (shape and engergy position) of Mn peaks between commercial MnO_2 and referecne MnO_2. Probably because the synthetic methods of MnO_2 for suppliers are various, which affect Mn's chemical environment.

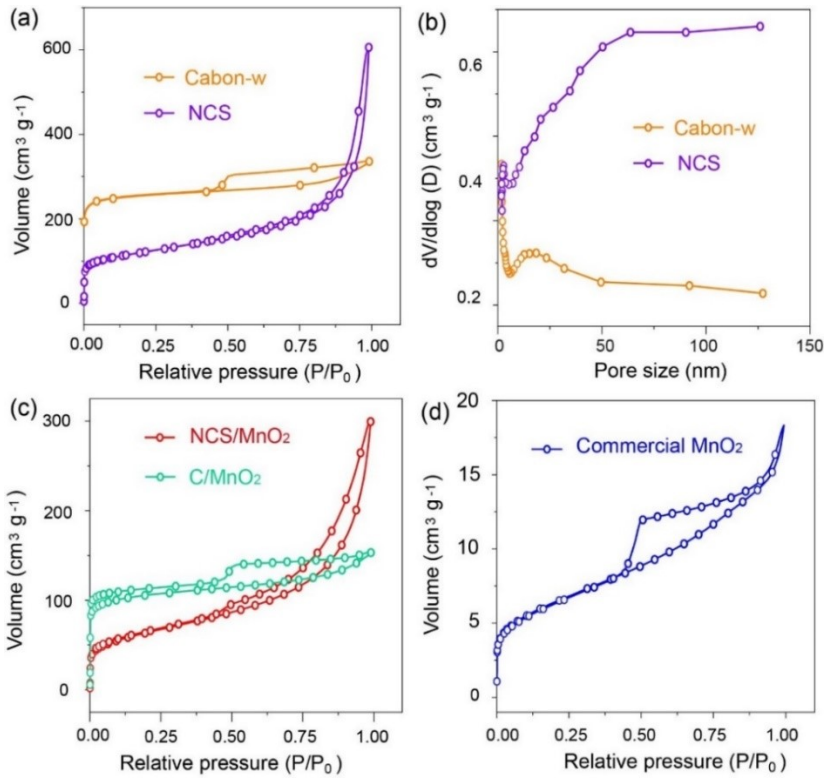

Fig. S4. (a) Nitrogen adsorption-desorption of NCS and carbon-w; (b) pore size distribution of NCS and carbon-w; (c) nitrogen adsorption-desorption of NCS/MnO_2 and C/MnO_2; (d) nitrogen adsorption-desorption of commercial MnO_2.

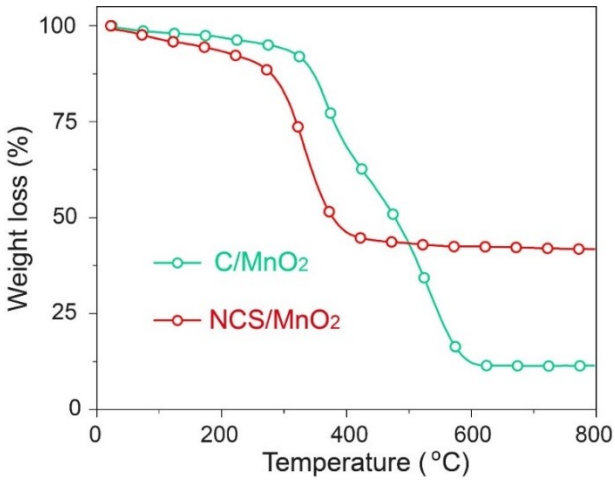

Fig. S5. TG curves of NCS/MnO_2 and C/MnO_2 in synthetic air flow.

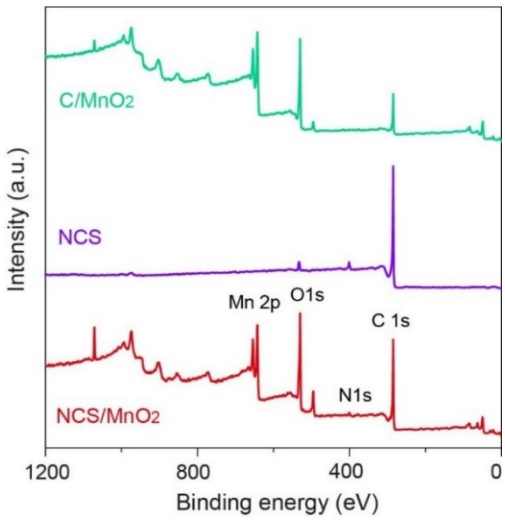

Fig. S6. Full XPS spectra of NCS/MnO_2, NCS and C/MnO_2

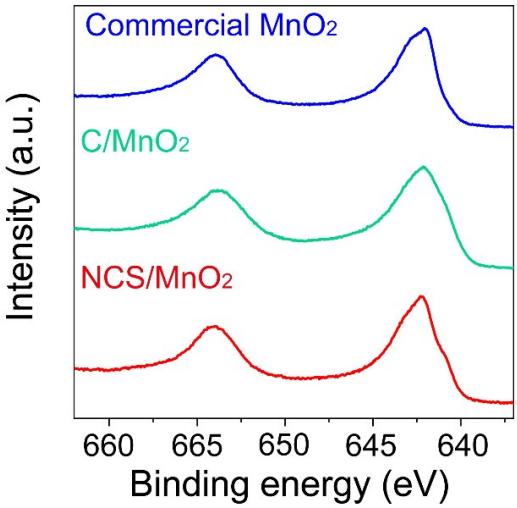

Fig. S7. Complete high-resolution XPS spectra of Mn 2p of of NCS/MnO_2, NCS and C/MnO_2.

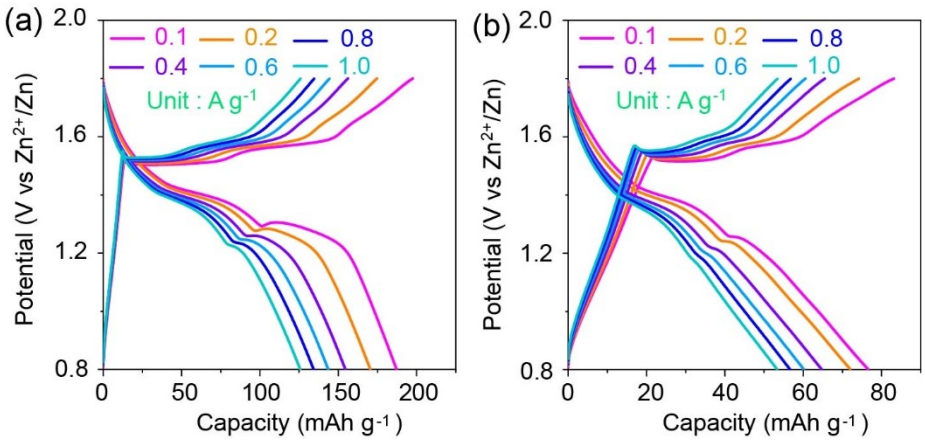

Fig. S8. Galvanostatic discharge/charge profiles of (a) Commercial MnO_2 and (b) C/MnO_2 at different current densities.

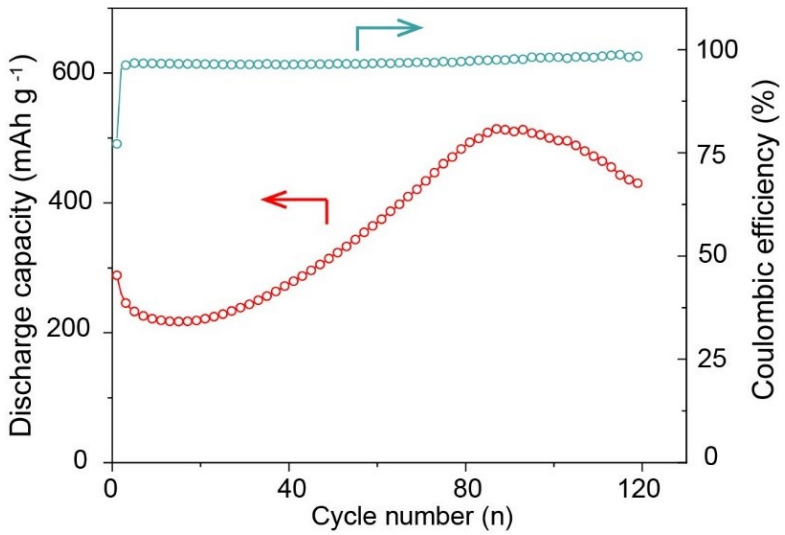

Fig. S9. Extended NCS/MnO_2 cycling performance at 0.2 A g^{-1}.

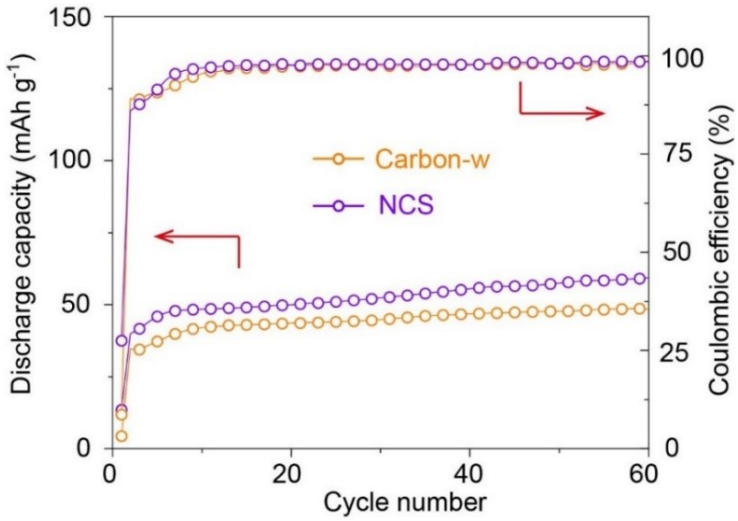

Fig. S10. Cycling performance of NCS and carbon-w at 0.2 A g^{-1}.

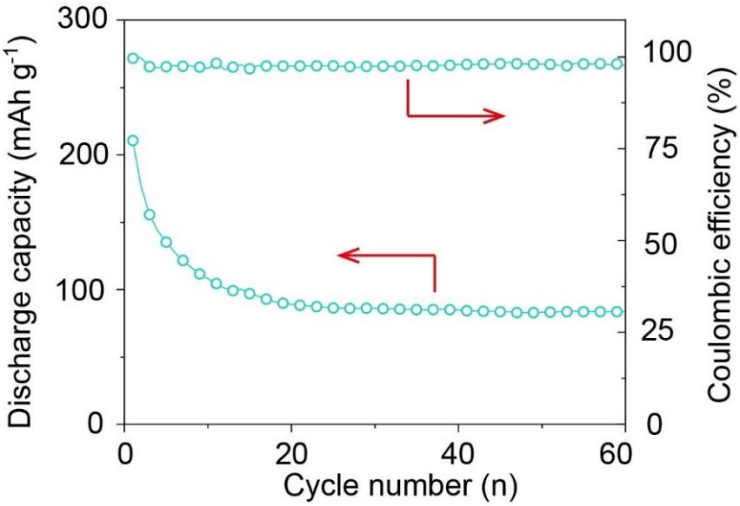

Fig. S11. Cycling performace of NCS/MnO_2 at 0.2 A g^{-1} with 2 M $ZnSO_4$.

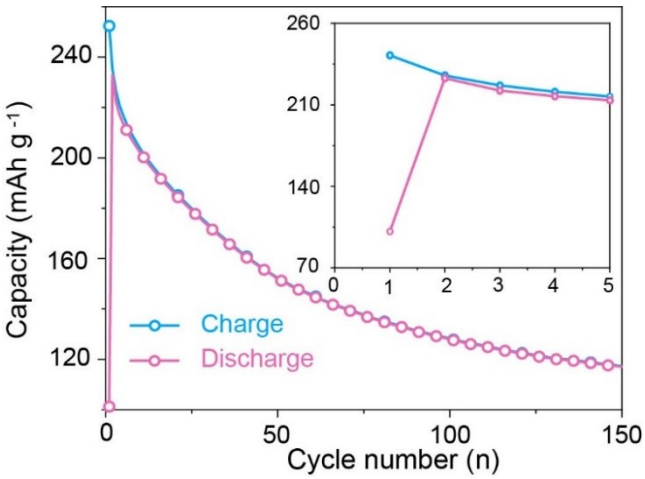

Fig. S12. The discharge and charge capacity of NCS/MnO_2 at 2 A g^{-1} during the early stage. Insert: druing the intial 5 cycles.

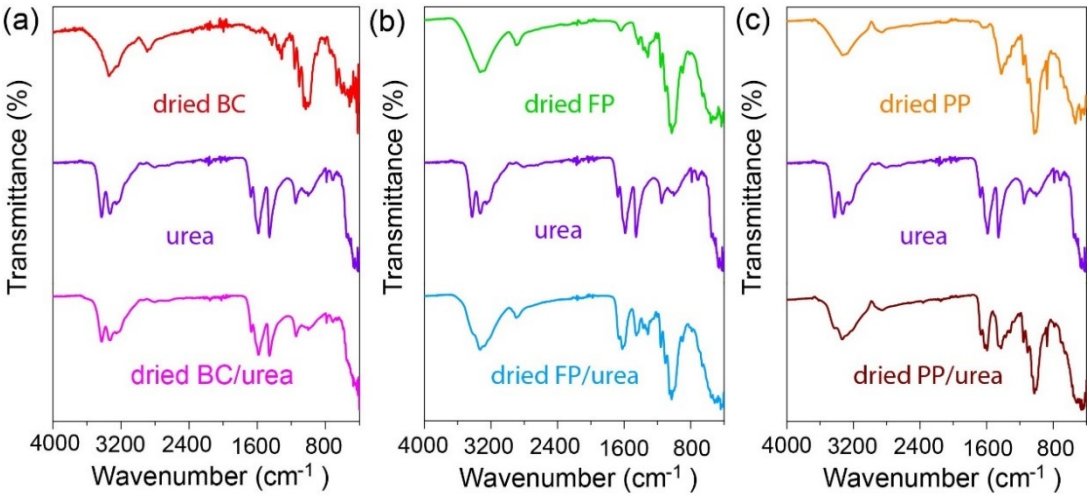

Fig. S13. FTIR of (a) dried BC, urea and dried BC/urea (b) dried FP, urea and dried FP/urea, (b) dried PP, urea and dried PP/urea

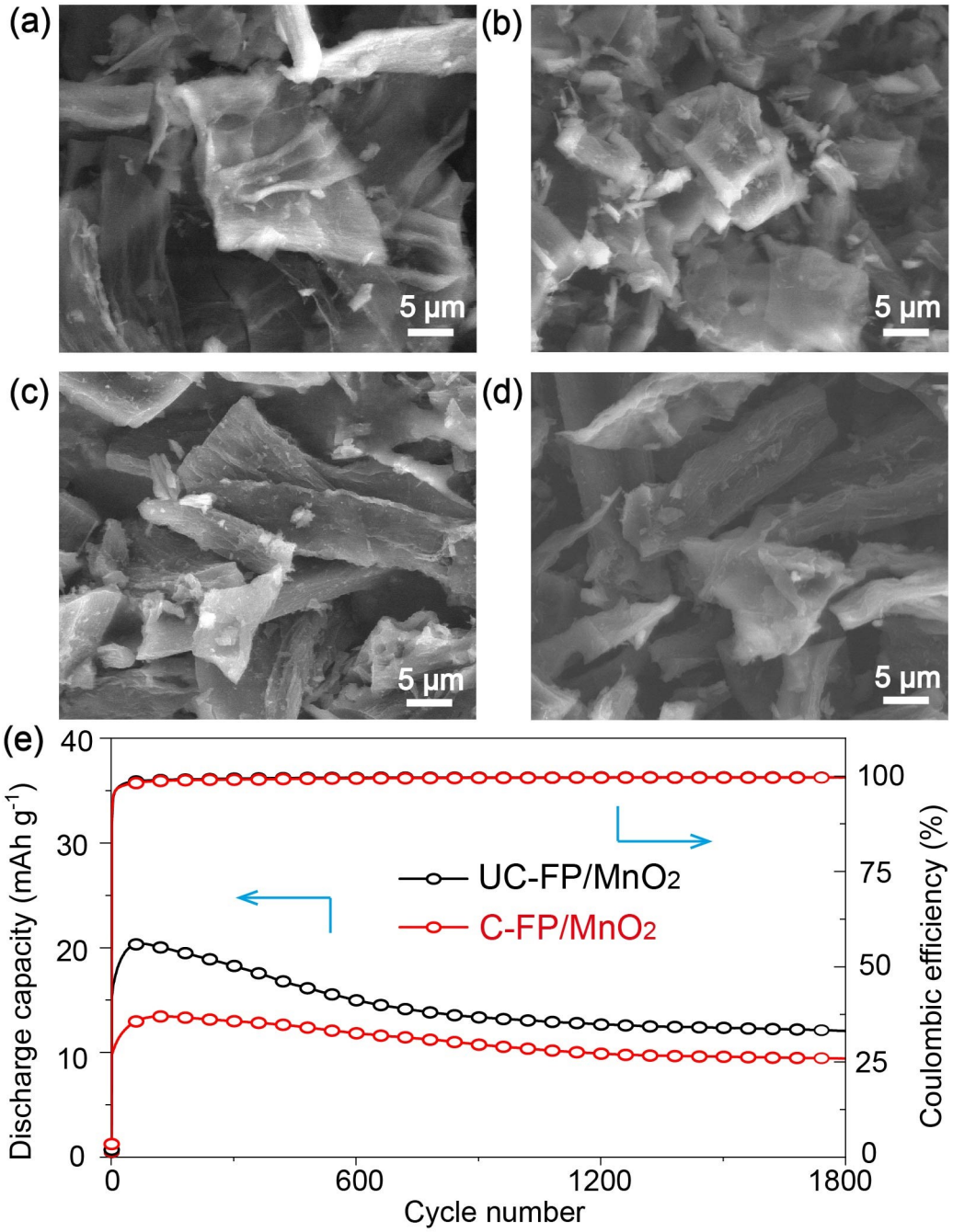

Fig. S14. Comparison of carbons from urea-treated (UC) and untreated (C) filter paper (FP). SEM images of (a) C-FP, (b) UC-FP, (c) C-FP/MnO_2 and (d) UC-FP/MnO_2. (e) Cycling performance of C-FP/MnO_2 and (d) UC-FP/MnO_2 at 2 A g^{-1}.

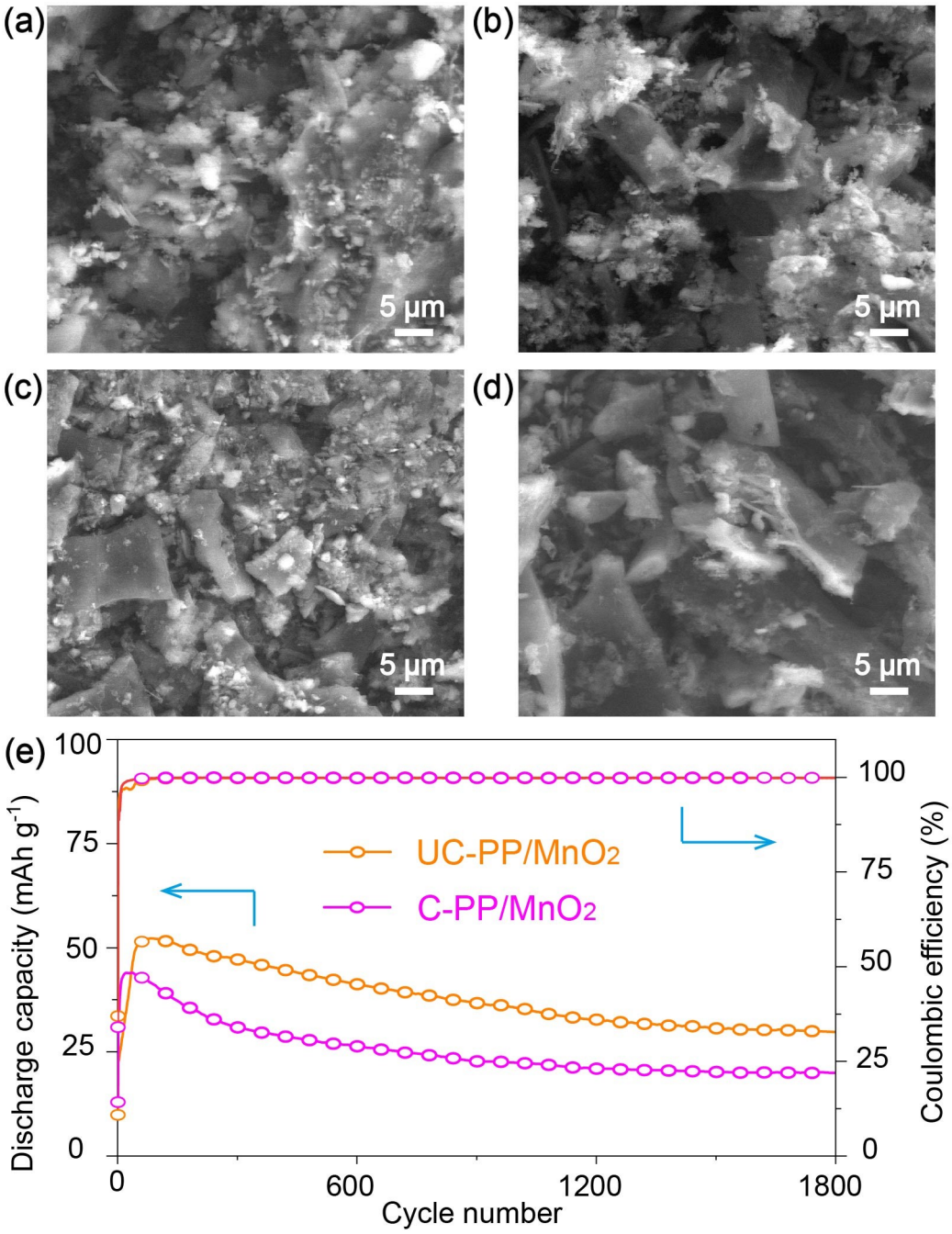

Fig. S15. Comparison of carbons from urea-treated (UC) and untreated (C) printer paper (PP). SEM images of (a) C-PP, (b) UC-PP, (c) C-PP/MnO_2 and (d) UC-PP/MnO_2. (e) Cycling performance of C-PP/MnO_2 and UC-PP/MnO_2 at 2 A g^{-1}.

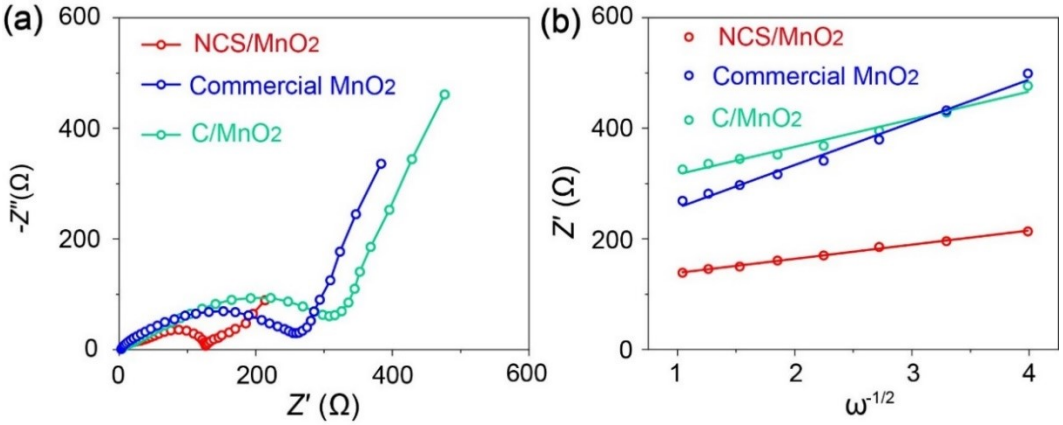

Fig. S16. (a) Nyquist plots at the open circuit voltage and (b) linear fits between Z′ and $w^{-1/2}$ for NCS/MnO_2, C/MnO_2 and Commercial MnO_2.

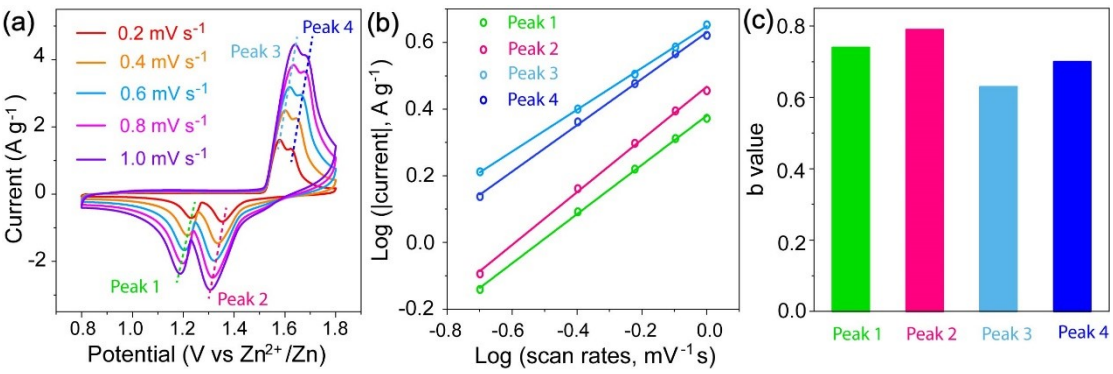

Fig. S17. (a) CV curves of NCS/MnO_2 at various scan rates. (b) relation between log *i* and log *v*. (c) the obtained b-values for the four peaks.

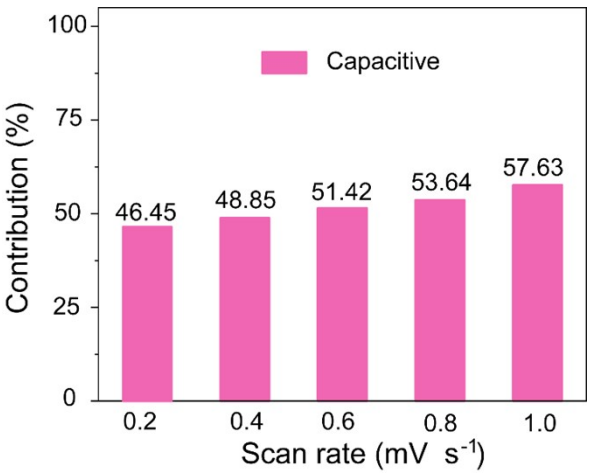

Fig. S18. Fractions of capacitive-like contributions to current for NCS/MnO_2 in CVs at different scan rates.

Generally the measured current (*i*) at a certain potential is consisted of the capacitive current (k_1v) and the diffusion current ($k_2v^{1/2}$) [1]: $i=k_1v+k_2v^{1/2}$. The value of k_1 and k_2 at a certain potential was obtained by fitting. The capacitive-like contribution is the integral area ratio between potential-k_1v curves and potential-*i* curves.

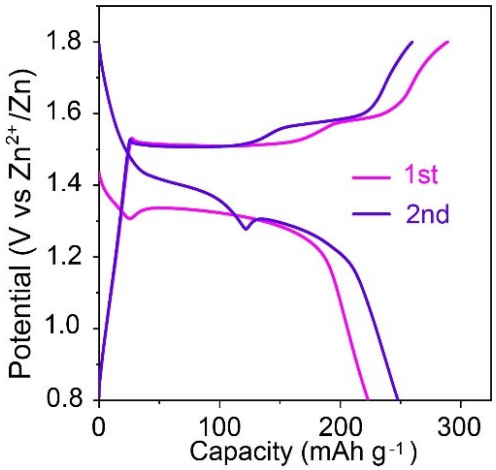

Fig. S19. Galvanostatic discharge/charge profiles of NCS/MnO_2 during the initial two cycles at 0.2 A g^{-1}.

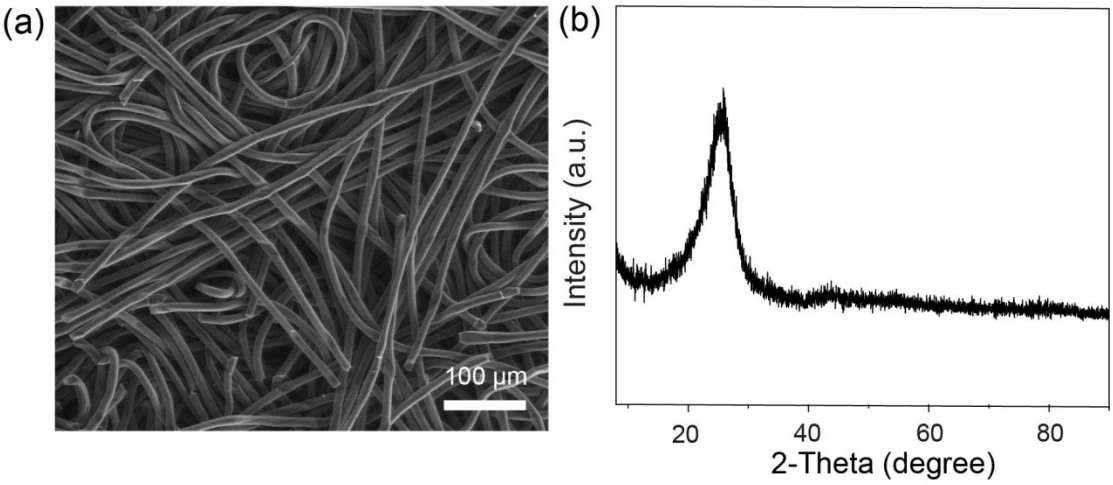

Fig. S20. (a) SEM image and (b) XRD pattern of bare carbon paper.

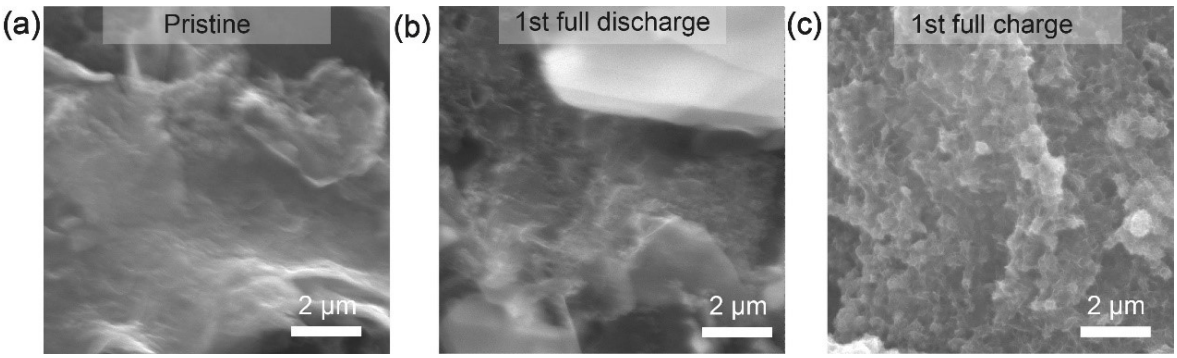

Fig. S21. SEM images of the 1st cycle for NCS/MnO_2.

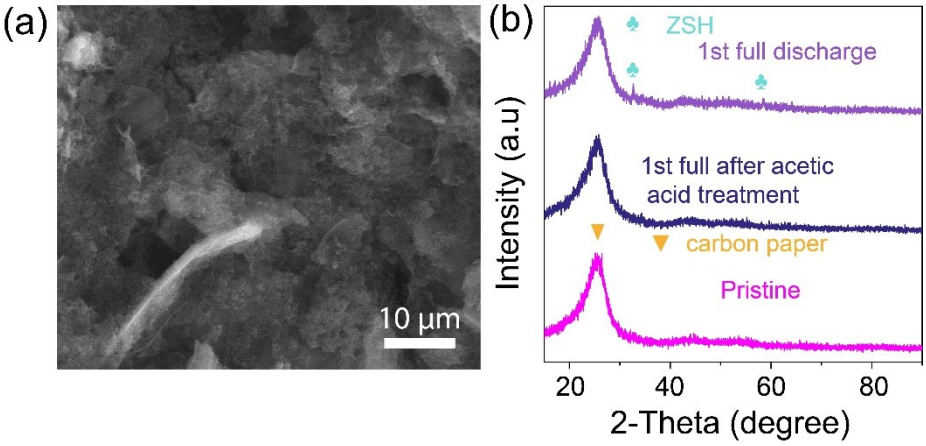

Fig. S22. SEM of the 1st discharge to 0.8 V of the NCS/MnO_2 electrode after acetic acid treatment (a); and comparison of XRD patterns (b).

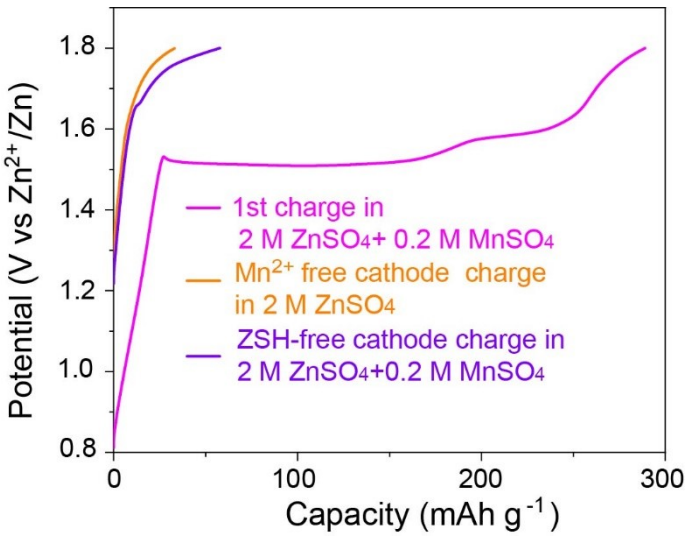

Fig. S23. Charge profiles for NCS/MnO_2 in presence of different chemical species.

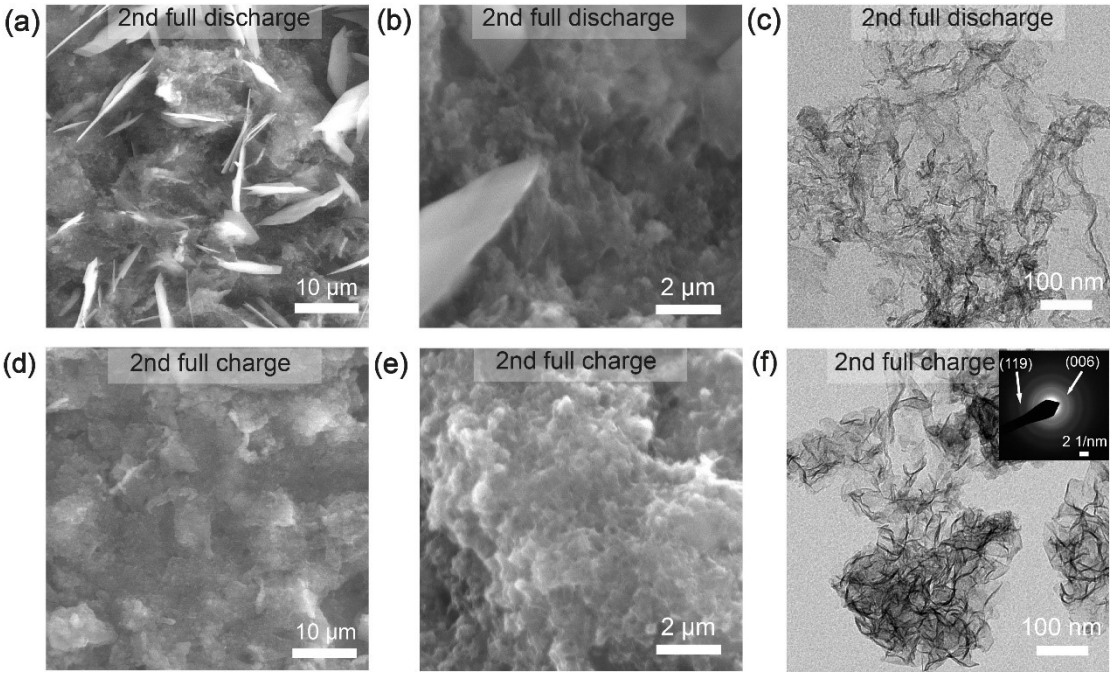

Fig. S24. SEM and TEM images at the 2nd cycle for NCS/MnO_2.

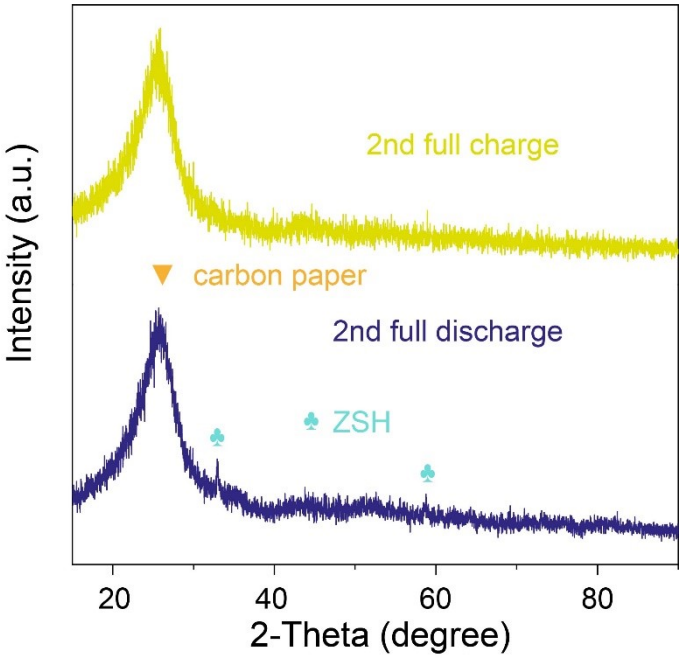

Fig. S25. XRD patterns of the 2nd cycle for NCS/MnO_2 at 0.2 A g^{-1}.

Table S1. Textural data of samples.

Samples	BET surface area (m^2 g^{-1})	External surface area (m^2 g^{-1})	Pore volume (cm^3 g^{-1})
Carbon-w [2]	1009	153	0.19
NCS	431	269	0.86
C/MnO_2	401	112	0.12
NCS/MnO_2	229	183	0.42
Commercial MnO_2	23	20	0.02

Table S2. Fraction of Mn^{3+} component with respect to the total Mn $2p_{3/2}$ area measured by XPS. Fits were obtained by adopting for Mn^{3+} and Mn^{4+} the multiplet shapes obtained by Ilton et al. [3]. For all components of both multiplets the same intensities and relative binding energies were maintained as reported in Ref. 2, and a fixed Gauss/Lorentz mixing factor of 0.5 was used.

Samples	NCS/MnO_2	C/MnO_2	Commercial MnO_2
Mn^{3+} fraction	0.60	0.91	0.26

Table S3. Comparison the cycling performance between NCS/MnO_2 and reported cathodes for aqueous zinc ion batteries.

Cathode	Cycling performance	References
NCS/MnO_2	114 mAh g^{-1} at 2 A g^{-1} after 1800 cycles	This work
MnOx@N-C	100 mAh g^{-1} at 2 A g^{-1} after 1600 cycles	*Adv Energy Mater*. 2018, **8** 1801445.
carbon coated MnO	116 mAh g^{-1} at 1 A g^{-1} after 1500 cycles	*Energy Storage Mater*. 2020, **24**, 394-401.
Co-Mn_3O_4/carbon nanosheet array	103 mAh g^{-1} at 2 A g^{-1} after 1100 cycles	*Adv Energy Mater*. 2021, **11**, 2003203
$ZnMn_2O_4$ microrods	49 mAh g^{-1} at 2 A g^{-1} after 1000 cycles	*Energy Storage Mater*. 2020, **28**, 407-417.
MoS_2	102 mAh g^{-1} at 0.5A g^{-1} after 600 cycles	*Energy Storage Mater.* 2019, **16**, 527-534.
Ocu-Mn_2O_3	112 mAh g^{-1} at 1 A g^{-1} after 600 cycles	*ACS Appl Mater Interfaces.* 2020,**12,** 28199
$Na_{0.44}MnO_2$	~37 mAh g^{-1} at 1 A g^{-1} after 800 cycles	*ACS Sustainable Chem Eng.* 2020, **8,** 10673-10681.
$Zn_3V_2O_7(OH)_2 \cdot 2H_2O$	101 mAh g^{-1} at 0.2 A g^{-1} after 300 cycles	*Adv Mater.* 2018, **30**, 1705580.
α-(Mn_2O_3–MnO_2)-500	95 mAh g^{-1} at 2 A g^{-1} after 800 cycles	*ACS Appl Mater Interfaces*. 2020, **12**, 32526-32535.

Table S4. Masses of different substrates and urea absorbed after drying

Substrate	BC	FP	PP
Absorbed urea mass (g cm^{-2})	0.15	0.004	0.005
Bare substrates (g cm^{-2})	0.006	0.009	0.008
Mass ratio between the absorbed urea/the bare substrate	25	0.4	0.6

Reference

1 S. Bi, Y. Wu, A. Cao, J. Tian, S. Zhang and Z. Niu, *Mater. Today Energy*, 2020, **18**, 100548.

2 W. Wang, S. Khabazian, S. Roig-Sanchez, A. Laromaine, A. Roig and D. Tonti, *Renew. Energ.*, 2021, **177**, 209-215.

3 E. S. Ilton, J. E. Post, P. J. Heaney, F. T. Ling and S. N. Kerisit, *Appl. Surf. Sci.*, 2016, **366**, 475-485.